metals

MDPI

Article

Effect of Nb Addition on the Phase Stability, Microstructure, and Mechanical Properties of Powder Metallurgy Ti-5Fe-xNb Alloys

Balakrishnan Manogar, Fei Yang and Leandro Bolzoni *

School of Engineering, The University of Waikato, Hamilton 3240, New Zealand
* Correspondence: bolzoni.leandro@gmail.com

Abstract: Ti alloys contemplating the simultaneous addition of Fe and Nb are available in the literature as Fe enhances the strength and Nb improves the biological behaviour of Ti. Nevertheless, casting has been the main manufacturing process, the Nb content is normally ≥10 wt.%, and no tensile properties are available. In this study, Ti-5Fe-xNb alloys (x = 2, 6, and 9 wt.%) were produced via powder metallurgy, which is more energy efficient than casting, with the aim of understanding the relationship between the mechanical behaviour and the microstructural changes brought about by the progressive addition of a greater amount of Nb. This study shows that the increment of the Nb content reduces the densification of the alloys, as the relative density decreases from 98.2% to 95.0%, but remarkably increases the volume fraction of the stabilised β phase (14→36%). Accordingly, the Ti-5Fe-xNb alloys are characterised by Widmanstätten microstructures, which become finer for higher Nb contents, and progressively higher mechanical properties including yield stress (725–949 MPa), ultimate tensile strength (828–995 MPa), and hardness (66.5–67.6 HRA), but lower elongation to fracture (4.0–5.1%). It is found that the ductility is much more influenced by the presence of the residual pores, whereas the strength greatly depends on the microstructural changes brought about by the addition of the alloying elements.

Keywords: titanium alloys; powder metallurgy; blending elemental; press and sinter; mechanical properties

Citation: Manogar, B.; Yang, F.; Bolzoni, L. Effect of Nb Addition on the Phase Stability, Microstructure, and Mechanical Properties of Powder Metallurgy Ti-5Fe-xNb Alloys. *Metals* **2022**, *12*, 1528. https://doi.org/10.3390/met12091528

Academic Editor: Francisco Paula Gómez Cuevas

Received: 16 August 2022
Accepted: 9 September 2022
Published: 15 September 2022

1. Introduction

The conventional choice of materials for structural implants has been stainless steel and Co-Cr alloys. However, these alloys posed severe threat as they have been found to be carcinogenic [1]. Hence, Ti alloys have been regarded as an effective alternative as they are known for their superior biocompatibility, excellent corrosion resistance [2,3], and high strength compared to other metals [4]. Further, Young's modulus of Ti alloys is the lowest when compared to other metallic biomaterials. Ideally, Young's modulus of an implant should be as close as possible to that of the human bone (10–30 GPa) [5] to avoid the stress shielding effect where the implant tends to bear a higher load than the adjacent bone. This results in the resorption of the adjacent bone, a phenomenon known as aseptic loosening [6]. Current Ti-based materials used in biomedicine are Ti and the Ti-6Al-V alloy. Their main limitations are not high enough strength for structural implants and the release of cytotoxic/neurotoxic metallic ions, respectively. Specifically, recent reports of toxic Al^+ and V^+ ions being released into the bloodstream have been linked to severe cases of neurodegenerative disorders such as Alzheimer's disease [7]. Consequently, researchers have focused on producing Al and V free alloys, viz. Ti-15Mo [8], Ti-29Nb-13Ta-4.6Zr [9], Ti-Mn [10], and various other alloys have been developed as an alternative to conventional Ti alloys [11].

The characteristic allotropic nature of Ti provides the flexibility of designing new alloys with enhanced mechanical and biological performance through microstructural

control. In particular, the alloying elements added to Ti are classified into α-stabilisers (Al, O, N, etc.), β-stabilisers (V, Mo, Nb, Fe, etc.), and neutral (Sn and Zr). These elements will increase, decrease, or slightly affect the allotropic phase transformation, known as β transus, contributing to the stabilisation of either the low temperature hcp α or the high temperature bcc β phase [12,13]. Beyond a critical composition (β_c), the β phase can be fully stabilised at room temperature. For instance, the β_c value for Mo is approximately 10 wt.%, meaning that adding 10 wt.% of Mo to Ti results in a fully stable β structure at room temperature. The stabilising power of the different alloying elements is commonly taken into account by means of the Molybdenum Equivalent (MoE) parameter [14]. Based on literature, an MoE $\geq$ 15 is required to produce fully stable β Ti alloys whilst α + β alloys Ti alloys are obtained for 8 $\leq$ MoE $\leq$ 15. However, as reported hereafter, in literature there are at least two different equations proposed to calculate the MoE parameter [15,16], where the weighting factors were obtained in quenched alloys:

$$\text{MoE} = 1.0\,[\text{Mo}] + 0.67\,[\text{V}] + 0.28\,[\text{Nb}] + 2.9\,[\text{Fe}] + 0.77\,[\text{Cu}] + 1.11\,[\text{Ni}] + 1.54\,[\text{Mn}] \quad (1)$$

$$\text{MoE} = 1.0\,[\text{Mo}] + 1.25\,[\text{V}] + 0.28\,[\text{Nb}] + 1.93\,[\text{Fe}] + 1.54\,[\text{Cu}] + 2.46\,[\text{Ni}] + 2.26\,[\text{Mn}] \quad (2)$$

Fe and Nb are two ideal alloying elements to develop Ti alloys. In particular, Fe is one of the strongest β-stabilisers (see MoE parameter's equations) with high diffusivity in Ti. Therefore, literature on the addition of Fe to Ti was primarily developed using powder metallurgy [17–19], where the addition of Fe enhances the densification and improves the mechanical properties of Ti. The addition of Fe to Ti while using casting has been far less studied [20] as a consequence of the higher density of Fe, which tends to sediment during solidification. Conventionally, the amount of Fe is limited to less than 7 wt.% to avoid the formation of TiFe-based intermetallic phases. The addition of Nb to Ti is documented in the literature as Nb is a non-toxic biocompatible element that increases surface acidity, stimulates cells' processes, and reduces electro-kinetic potential, thus promoting cell adhesion and proliferation [21]. Moreover, favourable attachment, proliferation, and differentiation of L929 and MG-63 cells in the cast of Ti-45Nb alloy have been reported as a satisfactorily cytotoxic evaluation [22]. Casting has been the main manufacturing route for Ti-Nb alloys, where the Nb content was varied between 5 wt.% and 35 wt.% to study the microstructural evolution and the associated performance [23–26]. Despite their intrinsic advantages such as less waste and higher energy efficiency, fewer studies considered powder metallurgy as a manufacturing method, and exclusively compositions with high Nb additions (i.e., $\geq$10 wt.%) were reported [27–29]. Regarding Ti-Fe-Nb alloys, few studies are available [30–34], where the primary limitations are that no tensile properties have been reported. The amount of Nb is generally $\geq$10 wt.% [31–34] and the advantages of powder metallurgy have not been exploited.

Therefore, the aim of this study is to understand the relationship between the mechanical behaviour, tensile properties in particular, of Ti-5Fe-xNb alloys and the changes induced by the increment of the Nb content (i.e., x = 2, 6 and 9 wt.%), which is kept below 10 wt.%. Consequently, the changes in physical properties, phase constitution, and microstructural evolution are linked to the mechanical behaviour. The Ti-5Fe-xNb alloys are designed, using Equations (1) and (2), to be processed via powder metallurgy to exploit its intrinsic benefits.

2. Materials and Methods

2.1. Raw Materials

The characteristics of the elemental Ti, Fe, and Nb powders used as starting materials in this study are shown in Table 1. Figure 1 displays the SEM micrographs of their morphology, which is, irregular, spherical, and angular. The size and morphology of each elemental powder has been chosen to favour good mechanical interlocking and sinterability, which are highly dependent on the powders' features [18,35].

Table 1. Characteristics of the elemental powders used in this study as per supplier's specifications.

Element	Max Particle Size	Purity (%)	Supplier
Titanium	200 mesh (<75 μm)	99.4	Goodfellow Ltd., Huntingdon, UK
Iron	1250 mesh (<10 μm)	99.0	Goodfellow Ltd., Huntingdon, UK
Niobium	325 mesh (<45 μm)	99.8	Alfa Aesar, Auckland, NZ

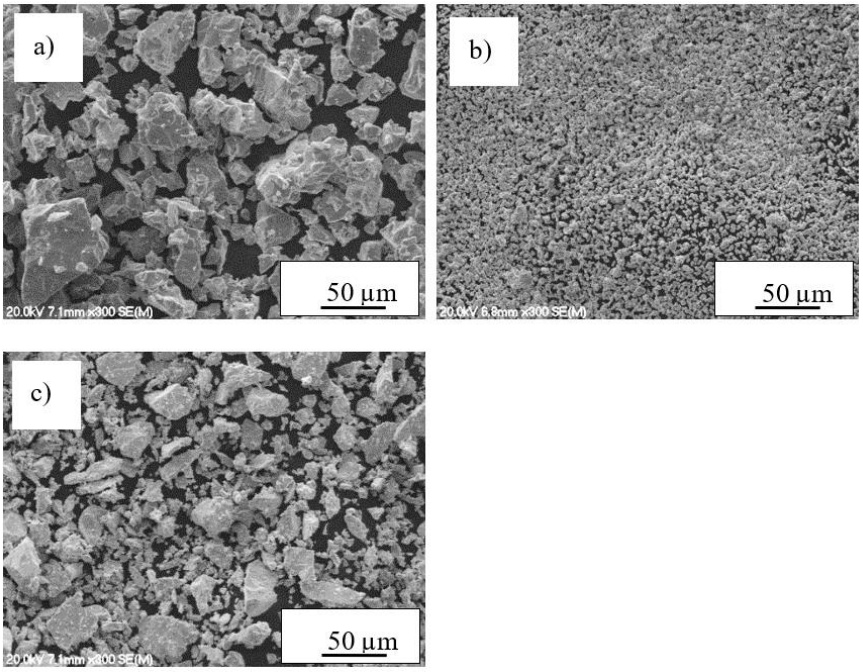

Figure 1. SEM micrographs of the elemental powders: (**a**) irregular Ti, (**b**) spherical Fe, and (**c**) angular Nb.

2.2. Processing Route

The Ti-based alloys studied (i.e., Ti-5Fe-xNb) had a constant Fe content (i.e., 5 wt.%) and a variable Nb content (i.e., 2, 6, and 9 wt.%). The respective powder blends were homogenised in the V-mixer at a frequency of 45 Hz for 30 min at room temperature prior to uniaxial warm pressing using a 100-ton hydraulic press at 600 MPa at a temperature of 200 °C. Warm pressing was chosen over cold pressing aiming to achieve high green density values in the cylindrical samples of 40 mm diameter and approximately 18 mm height. It is worth mentioning that no lubricant was intentionally added to reduce contamination, but the walls of the die were lubricated with a graphitic coating. The green bodies were heated up to 1300 °C in a vacuum furnace (ZSJ—20 × 20 × 30) and isothermally held for 2 h for sintering. The vacuum level was set to 10^{-3} Pa, and the heating and cooling rates were set to 10 °C/min.

2.3. Characterisation

The theoretical density of the alloys was calculated using the rule of mixtures. The green density of the compacts (ρ_g) was calculated using the mass, which was measured using an analytical scale, and the volume. The density of the sintered samples (ρ_s) was measured using the Archimedes' principles. Relative density values were computed by dividing the measured values by the theoretical density of the alloy. Densification (Ψ), which is defined as the ratio of actual change in density to the expected change in density during sintering [35], was calculated using Equation (3):

$$\Psi = \frac{(\rho_S - \rho_G)}{(1 - \rho_G)} \times 100 \quad (3)$$

XRD was performed using a Philips X'pert diffractometer (Philips, Amsterdam, The Netherlands) with Cu K_α radiation operated at 45 kV and 40 mA. An Olympus BX60 optical microscope, equipped with Nikon digital camera (DS-SMc) and a field emission Hitachi S4700 scanning electron microscope (Hitachi, Tokyo, Japan), were used for the metallographic characterisation. For that, the samples were ground using #320, #600, and #1000 grit silicon carbide grinding papers prior to using a Struers Tegramin-25 semi-automatic polisher (Struers, Copenhagen, Denmark). A non-drying colloidal silica suspension was used as the polishing solution. In order to perform the microstructural characterisation, the samples were etched using Kroll's reagent (4% Hydrofluoric acid, 5% Nitric acid, and 91% distilled water). Uniaxial tensile testing, at least three tensile tests per composition, was performed on an INSTRON 33R 4204 universal testing machine (Instron, Norwood, MA, USA). The cross-head speed was set to 0.1 mm/min. An INSTRON static axial strain gauge extensometer with a gauge length of 10 mm was used to obtain the elongation. The samples were cut into dog-bone shaped tensile samples with a gauge length of 20 mm. Five independent Rockwell hardness (HRA) measurements (LECO Corp., St. Joseph, MI, USA) were performed to calculate the average hardness of the Ti-5Fe-xNb alloys.

3. Results and Discussion

3.1. Density and Porosity

Table 2 shows the relative green and sintered density values of the Ti-5Fe-xNb alloys along with the values of the MoE parameters as calculated by means of Equations (1) and (2). It can be seen that the green density decreases with the amount of Nb added, due to the higher hardness, which is related to the compressibility of the Nb powder particles compared to Ti and Fe. A 2.5% decrease in green density is observed with the addition of Nb from Ti-5Fe-2Nb to Ti-5Fe-6Nb with a further decrease of 0.7% for Ti-5Fe-9Nb. Consequently, the values of the relative sintered density also decrease with the increment of Nb with a decrease of 1.8% and 1.4% as the content of Nb increases from 2 wt.% to 6 wt.%, and to 9 wt.%. Sintering of the samples leads to their densification with an average gain in relative density of 3.9 $\pm$ 0.1% reaching values in the 95–98% range, which is typical of powder metallurgy Ti-based materials [27,36]. Therefore, Ti-5Fe-2Nb has the highest relative green and sintered density, which should correspond to the highest densification value, whereas Ti-5Fe-9Nb has the lowest values. As expected, higher values of the MoE parameter are achieved with the progressive addition of Nb, and Equation (2) results in proportionally lower values compared to Equation (1), due to the lower weighting factor of Fe.

Table 2. Values of the relative green and sintered density, and associated MoE parameters, of the Ti-5Fe-xNb alloys compared to Ti-5Fe. Ti-5Fe data from ref. [37].

Alloy	Green Density (%)	Sintered Density (%)	MoE (Equation (1))	MoE (Equation (2))
Ti-5Fe [37]	88.0	97.0	15	9.7
Ti-5Fe-2Nb	93.8	98.2	15.5	10.2
Ti-5Fe-6Nb	91.3	96.4	16.6	11.3
Ti-5Fe-9Nb	90.6	95.0	17.5	12.2

Figure 2 shows the relationship between densification and porosity of the Ti-5Fe-xNb alloys as a function of the Nb content. It can be seen that with the addition of Nb the densification of the Ti-5Fe-xNb alloys gradually decreases while the porosity increases as both depend on the features of the initial powders, the green density, and the sintering conditions [28]. Specifically, Nb has a high melting point and is, therefore, the element slowing down the densification of the Ti-5Fe-xNb alloys. For instance, a sintering temperature of 1500 °C was needed to be able to achieve ~5% of porosity (i.e., 95% relative density) in binary Ti-Nb alloys [27]. Romero et al. [37] produced the Ti-5Fe alloy by warm compacting Ti and Fe powders with similar size and morphology to the ones used in the current study.

However, uniaxial compaction was done at 400 MPa, which resulted in a slightly higher porosity when compared to Ti-5Fe-2Nb (Figure 2). It can be noticed that due to the absence of Nb, a higher densification was achieved in the Ti-5Fe alloy as the low melting point and high diffusivity of Fe favour densification.

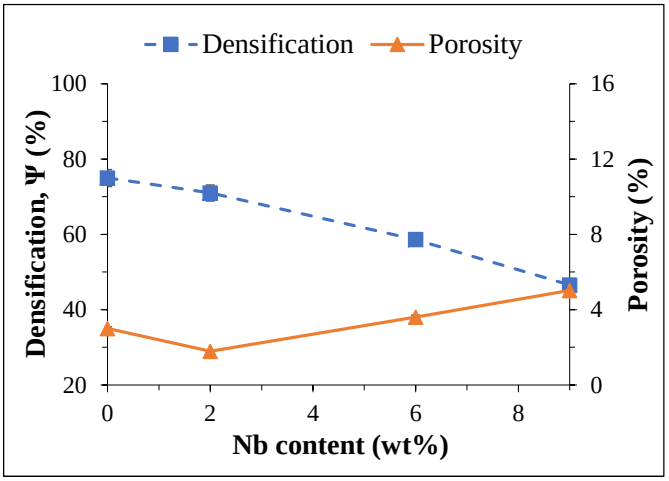

Figure 2. Relationship between densification and porosity as a function of the Nb content. Ti-5Fe data from ref. [37].

3.2. Phase and Microstructural Analysis

From the XRD spectra shown in Figure 3, it can be seen that the hcp α and bcc β phases are the main phases composing the Ti-5Fe-xNb alloys. Ti-5Fe-2Nb has the lowest amount of β phase, which then increases for the higher amount of Nb as reflected by the higher relative intensities of the β phase peaks of Ti-5Fe-6Nb and Ti-5Fe-9Nb. It is worth noticing that the presence of a small amount of α″ phase was also detected in Ti-5Fe-9Nb, which has been previously reported for Ti alloys containing a high amount of Nb [38]. The metastable ω phase in arc melted and vacuum suction cast Ti-3Fe-10Nb and Ti-3Fe-15Nb were detected by Chaves et al. [34]. The α′ phase in cast Ti-5Nb-1Fe and Ti-5Nb-2Fe and the ω phase in cast Ti-5Nb-2Fe and Ti-5Nb-3Fe was detected by Hsu et al. [30]. Lee et al. [24] showed that Ti-Nb alloys with less than 15 wt.% Nb are characterised by the presence of a distorted hexagonal structure α′. The formation of the α″ phase in Ti-7Fe-xNb alloys has also been reported during quenching of the samples as a result of the high cooling rate [39].

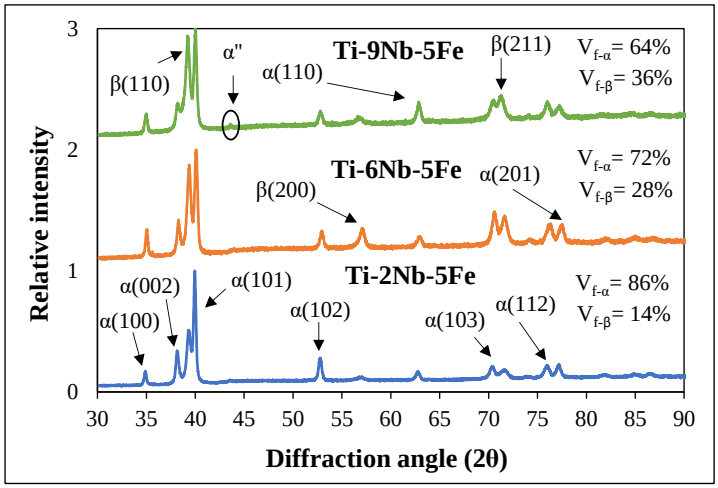

Figure 3. XRD spectra of the Ti-5Fe-xNb alloys.

The differences in phases detected are related to both the composition and the processing conditions where casting is generally characterised by higher cooling rates than sintering. Quantification of the volume fraction of the α ($V_{f\text{-}\alpha}$) and β ($V_{f\text{-}\beta}$) phases from the XRD spectra of Figure 3 indicated that $V_{f\text{-}\beta}$ increases from ~14% to ~28% and then to ~36% as the amount of Nb is increased from 2 wt.% to 6 wt.% and then to 9 wt.%. Based on the XRD patterns and the volume fraction data, it can be stated that all Ti-5Fe-xNb alloys can be regarded as α + β or metastable β alloys.

Figure 4 shows the optical and SEM micrographs of the Ti-5Fe-xNb alloys where it can be seen that all alloys are characterised by Widmanstätten microstructures [40]. As the amount of Nb added is increased, prior β grains of comparable size are found within the alloys as seen from the optical micrographs (Figure 4a,c,e). Moreover, a remarkable refinement of the size of the α + β lamellae as well as of the interlamellar spacing as a consequence of the greater amount of stabilised β phase is also obtained as seen from the SEM micrographs (Figure 4b,d,f). The microstructure of Ti-5Fe-2Nb and Ti-5Fe-6Nb is similar to that of Ti-10Nb and Ti-15Nb produced by vacuum pressure type casting system [24].

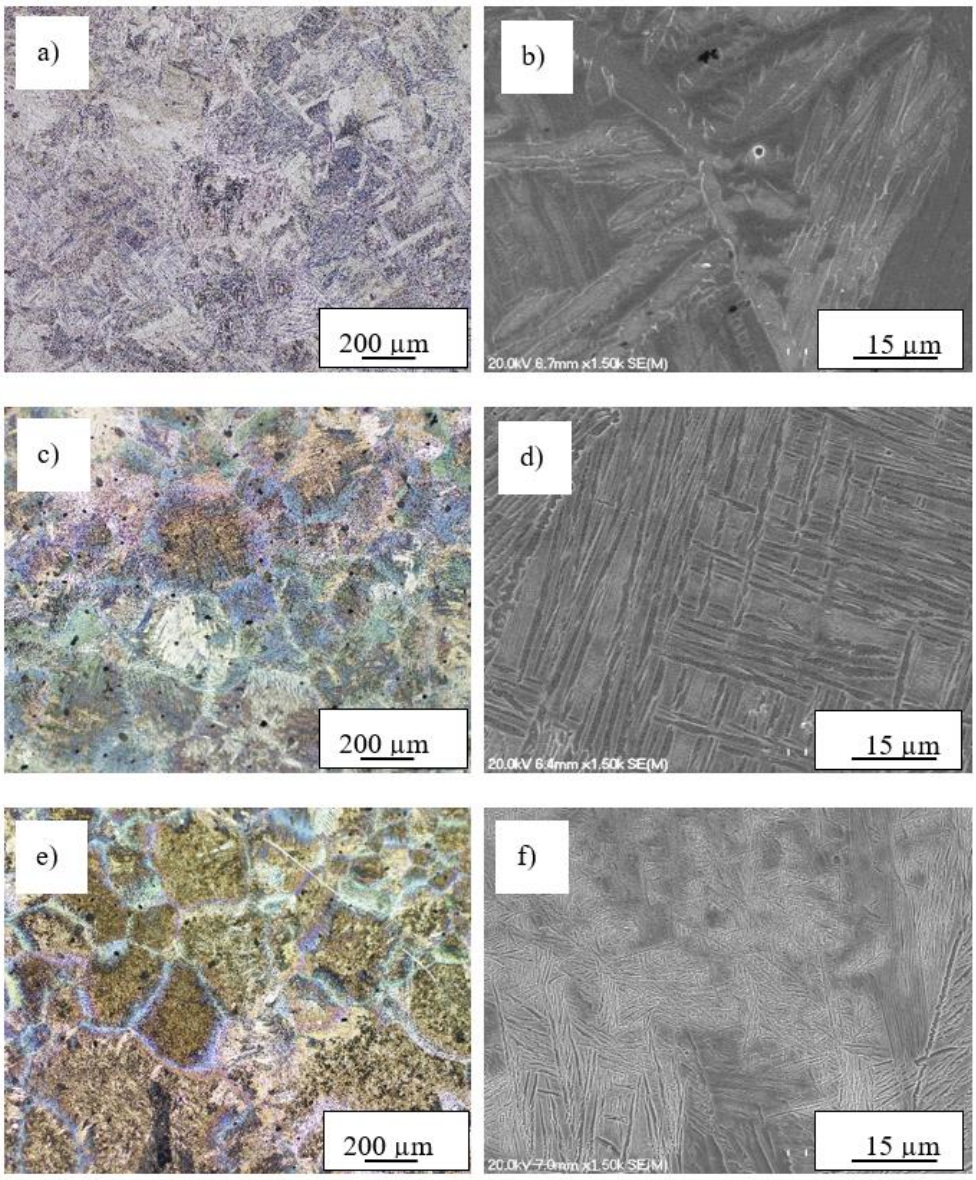

Figure 4. Optical and SEM micrographs, respectively, of the Ti-5Fe-xNb alloys: (**a**,**b**) Ti-5Fe-2Nb, (**c**,**d**) Ti-5Fe-6Nb, and (**e**,**f**) Ti-5Fe-9Nb.

Furthermore, the Ti-5Fe-xNb alloys have comparable microstructure to that of the Ti-10Nb and Ti-20Nb alloys produced by casting followed by furnace cooling to 600 °C and final air cooling to room temperature [23]. The results of the microstructural analysis of Figure 4 also show that a small amount of isolated spherically shaped residual pores are present in the microstructure of the Ti-5Fe-xNb alloys, which is typical of the last stage of sintering. The micrographs of Figure 4 also confirm that the Ti-5Fe-xNb alloys belong to the α + β or metastable β category as opposed to the fully stable β alloys as indicated by Equation (1), which could have been used aiming to create fully stable β Ti-5Fe-xNb alloys. Hence, it is worth mentioning that the MoE parameter from Equation (2) seems to be more accurate to design new Ti-based alloys via powder metallurgy, which is generally characterised by low cooling rates.

3.3. Mechanical Properties

Representative stress-strain curves of the Ti-5Fe-xNb alloys and the associated micrographs of the fracture surface are shown in Figure 5. A general increase in the tensile strength, both in terms of yield stress and ultimate tensile strength, results from the incremental addition of the Nb content, whereas the uniform elongation progressively decreases. The tensile curves of the Ti-5Fe-xNb alloys show both elastic as well as plastic deformation before non-catastrophic failure regardless of the chemical composition. Consequently, fractographic analysis mainly shows a ductile fracture surface. Specifically, the Ti-5Fe-xNb alloys fail through intergranular fracture along the α + β lamellae, which gives a rough dimple-like appearance, as well as intergranular fracture of the α grain boundaries. The latter leads to the formation of tear ridges, which become more pronounced as the amount of Nb in the Ti-5Fe-xNb alloys increases. It is worth noticing that dimples are also present in the fracture surface, especially for the Ti-2Fe-5Nb alloy. Comparable fracture surfaces to the Ti-5Fe-2Nb and Ti-5Fe-9Nb alloys were, respectively, reported by Zhao et al. [27] for the Ti-10Nb alloy produced by metal injection moulding and by Hsu et al. [30] for the Ti-2Fe-5Nb alloy manufactured via casting.

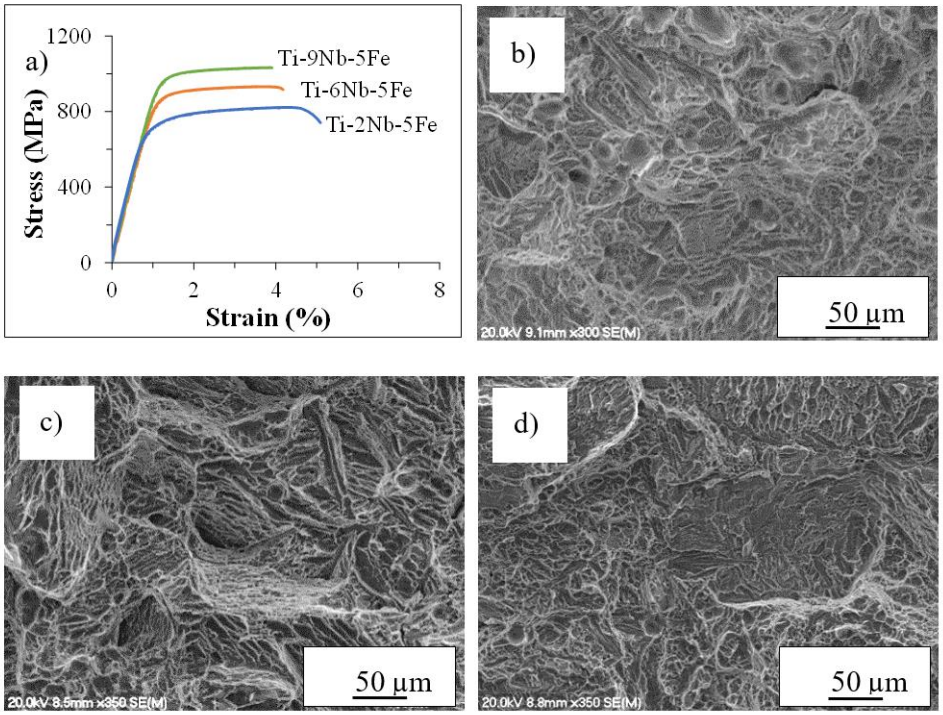

Figure 5. Representative tensile stress-strain curves (**a**) and micrographs (**b**–**d**) of the fracture surface of the Ti-5Fe-xNb alloys: (**b**) Ti-5Fe-2Nb, (**c**) Ti-5Fe-6Nb, and (**d**) Ti-5Fe-9Nb.

Figure 6 shows the average mechanical properties of the Ti-5Fe-xNb alloys as a function of the Nb content. In agreement with the representative stress-strain curves (Figure 5a), the yield stress and the ultimate tensile strength monotonically increase with the amount of Nb added, ranging between 725 ± 25 MPa and 949 ± 29 MPa, and 828 ± 14 MPa and 995 ± 13 MPa, respectively. Therefore, Ti-5Fe-2Nb and Ti-5Fe-9Nb show the lowest and highest tensile strength values. Consequently, the addition of Nb causes the hardness to increase linearly, and the ductility to decrease from 5.1 ± 0.4% to 4.0 ± 0.7%. Romero et al. [37] reported the ultimate tensile strength (i.e., 835 MPa) and elongation to fracture (2.1%) of the Ti-5Fe alloy produced by conventional powder metallurgy, which is also shown in Figure 6. This means that Ti-5Fe-2Nb has similar tensile strength, but higher ductility compared to the Ti-5Fe alloy as a result of the addition of Nb and the slightly higher relative density value (Table 1). The addition of 6 wt.% and 9 wt.% of Nb leads to a further increase in UTS of 17% and 30% compared to Ti-5Fe-2Nb.

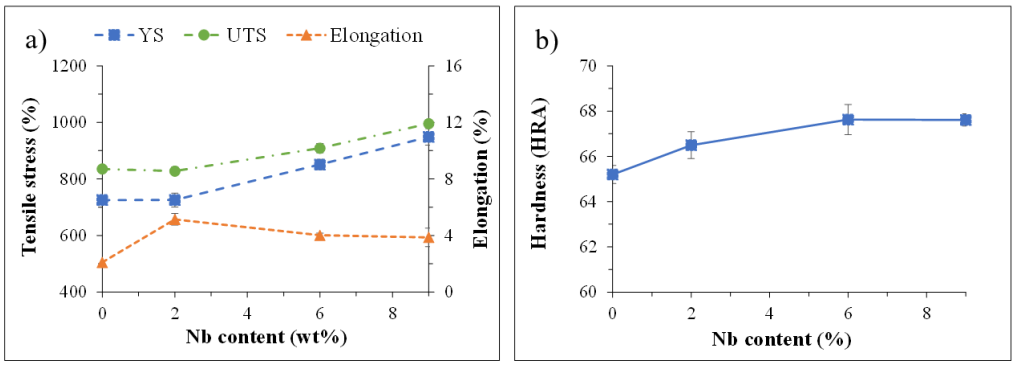

Figure 6. Average mechanical properties of the Ti-5Fe-xNb alloys: (**a**) tensile properties, and (**b**) hardness. Ti-5Fe data from ref. [37].

The increment of the resistance to plastic deformation and the associated reduction of the ductility of the Ti-5Fe-xNb alloys shown in Figure 6 is the compromise between the different effects brought about by the addition of Nb. Specifically, the higher the amount of Nb, the lower the relative sintered density and the finer the Widmanstätten microstructure due to greater $V_{f\text{-}\beta}$. A lower relative sintered density value means a greater amount of porosity within the microstructure, where pores reduce the load-bearing cross-section and constitute stress concentration sites [41], leading to a reduction of the tensile properties. A finer Widmanstätten microstructure means finer α + β lamellae as well as smaller interlamellar spacing and, thus, more boundaries hindering the movement of dislocations typical of grain refined structures [42]. In order to gain better insight on the actual factor controlling the mechanical behaviour, the average tensile properties of the Ti-5Fe-xNb alloys are, therefore, plotted in Figure 7 as a function of relevant parameters.

The variation of the tensile properties as a function of the relative density of the sintered Ti-5Fe-xNb alloys (Figure 7a) shows that the yield stress and the ultimate tensile strength decrease while the ductility increases as the amount of porosity decreases. This indicates that porosity has a greater impact on the ductility of the Ti-5Fe-xNb alloys rather than on their strength, as the latter is also meant to increase with the increment of the relative density. With respect to the variation of the tensile properties as a function of the MoE parameter (Figure 7b) and the $V_{f\text{-}\beta}$ (Figure 7c), the Ti-5Fe-xNb alloys become progressively stronger and less ductile. This is due to the solid solution strengthening induced by the presence of a greater amount of Nb atoms dissolved within the Ti lattice, as Nb has complete solubility in both the α and β phases, and the related microstructural changes. Specifically, the stabilisation of a greater amount of stronger β phase and the creation of increasingly finer lamellae with progressively smaller interlamellar spacing boosts the impediment of the movement of the dislocations.

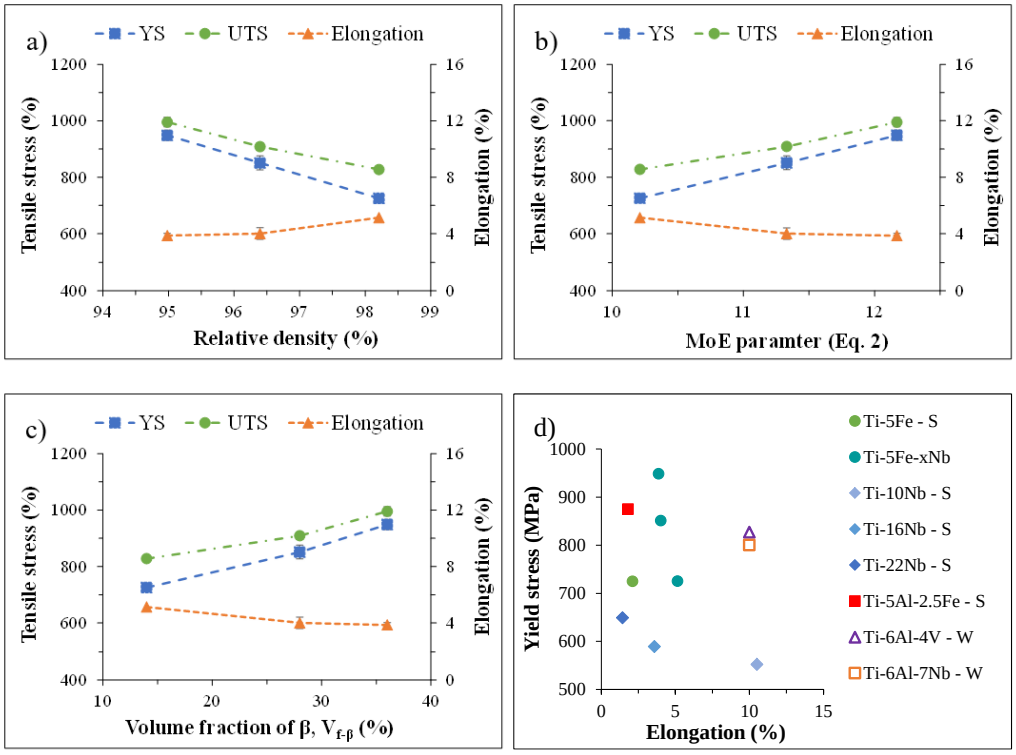

Figure 7. Average mechanical properties of the Ti-5Fe-xNb alloys as a function of the relative density (**a**), the MoE parameter as calculated by means of Equation (2) (**b**), and $V_{f-\beta}$, the volume fraction of phase β (**c**); and comparison of the yield stress/elongation pairs with literature (**d**) [27,37,43,44]. Legend: S-sintered, and W-wrought.

Figure 7d shows the comparison of the yield stress/elongation pairs of the Ti-5Fe-xNb alloys with the literature [27,37,43,44]. It can be seen that the Ti-5Fe-xNb alloys have better overall properties with respect to the sintered Ti-5Fe and Ti-5Al-2.5 alloys, although the latter has higher strength than Ti-5Fe-2Nb. In comparison to sintered Ti-xNb alloys (x = 10, 16, and 22 wt.%), the Ti-5Fe-xNb alloys have always much higher strength and better elongation, with the exception of the Ti-10Nb alloy. The higher strength is due to the strengthening contributions brought about by the presence of Fe. With respect to common wrought α + β alloys such as Ti-6Al-4V and Ti-6Al-7Nb, the Ti-5Fe-xNb alloys have higher strength, with the exception of Ti-5Fe-2Nb, but lower ductility. The latter is due to the expected higher amount of oxygen content derived by the use of a hydride-dehydride powder to produce the Ti-5Fe-xNb alloys as well as due to the presence of the residual pores left by the sintering process. If needed, the ductility could, therefore, be enhanced by post-processing the Ti-5Fe-xNb alloys by means of hot isostatic pressing or thermomechanical deformation processes aiming to seal the residual porosity.

4. Conclusions

Ti-5Fe-xNb alloys (x = 2, 6, and 9 wt.%) were successfully produced via the conventional powder metallurgy route. It was found that the addition of the elemental Nb powder decreases the deformability of the powder blend (i.e., lower green density), resulting in a linear decrease of the sintered density for higher Nb additions. Consequently, the densification of the Ti-5Fe-xNb alloys decreases, indicating that the slow diffusivity of Nb due to its high melting point is the primary factor limiting densification. The addition of Nb leads to the creation of alloys characterised by a Widmanstätten microstructure with the interlamellar spacing decreasing for higher Nb contents. Therefore, a general increase in the strength and the hardness associated with a decrease in the uniform elongation is found for higher Nb contents in the Ti-5Fe-xNb alloys. The alloys, consequently, fail through

intergranular fracture along the α + β lamellae combined with intergranular fracture of the α grain boundaries. Porosity has a greater impact on the ductility of the Ti-5Fe-xNb alloys rather than on their strength. The increase of the latter is directly related to the volume fraction of stabilised β phase ($V_{f\text{-}\beta}$) and so on to the MoE parameter. In general, the Ti-5Fe-xNb alloys have higher strength compared to other Fe- or Nb-bearing sintered binary alloys as well as wrought Ti alloys used in biomedicine.

Author Contributions: Conceptualization, B.M. and L.B.; methodology, B.M., F.Y. and L.B.; investigation, B.M.; resources, L.B.; data curation, B.M. and L.B.; writing—original draft preparation, B.M.; writing—review and editing, L.B.; supervision, L.B.; project administration, L.B. All authors have read and agreed to the published version of the manuscript.

Funding: This research was funded by the New Zealand Ministry of Business, Innovation and Employment (MBIE), UOWX1402 research contract.

Data Availability Statement: All metadata pertaining to this work will be made available on reasonable requests.

Acknowledgments: This work was supported by the New Zealand Ministry of Business, Innovation and Employment (MBIE) through the UOWX1402 research contract.

Conflicts of Interest: The authors declare no conflict of interest.

References

1. Szczęsny, G.; Kopec, M.; Politis, D.J.; Kowalewski, Z.L.; Łazarski, A.; Szolc, T. A review on biomaterials for orthopaedic surgery and traumatology: From past to present. *Materials* **2022**, *15*, 3622. [CrossRef] [PubMed]
2. Qi, P.; Li, B.; Wang, T.; Zhou, L.; Nie, Z. Microstructure and properties of a novel ternary Ti-6Zr-xFe alloy for biomedical applications. *J. Alloy Comp.* **2021**, *854*, 157119. [CrossRef]
3. Hein, M.; Kokalj, D.; Dias, N.F.L.; Stangier, D.; Oltmanns, H.; Pramanik, S.; Kietzmann, M.; Hoyer, K.-P.; Meißner, J.; Tillmann, W.; et al. Low cycle fatigue performance of additively processed and heat-treated Ti-6Al-7Nb alloy for biomedical applications. *Metals* **2022**, *12*, 122. [CrossRef]
4. Bolzoni, L.; Nowak, M.; Babu, N.H. Assessment of the influence of Al-2Nb-2B master alloy on the grain refinement and properties of LM6 (A413) alloy. *Mater. Sci. Eng. A* **2015**, *628*, 230–237. [CrossRef]
5. Chen, Q.; Thouas, G.A. Metallic implant biomaterials. *Mater. Sci. Eng. R* **2015**, *87*, 1–57.
6. Geetha, M.; Singh, A.K.; Asokamani, R.; Gogia, A.K. Ti based biomaterials, the ultimate choice for orthopaedic implants—A review. *Prog. Mater. Sci.* **2009**, *54*, 397–425.
7. Silva, H.; Schneider, S.; Neto, C.M. Study of nontoxic aluminum and vanadium-free titanium alloys for biomedical applications. *Mater. Sci. Eng. C* **2004**, *24*, 679–682. [CrossRef]
8. Chen, Y.Y.; XU, L.J.; LIU, Z.G.; KONG, F.T.; CHEN, Z.Y. Microstructures and properties of titanium alloys Ti-Mo for dental use. *Trans. Nonfer. Met. Soc. China* **2006**, *16*, s824–s828. [CrossRef]
9. Plaine, A.H.; da Silva, M.R.; Bolfarini, C. Tailoring the microstructure and mechanical properties of metastable Ti-29Nb-13Ta-4.6Zr alloy for self-expansible stent applications. *J. Alloy Comp.* **2019**, *800*, 35–40. [CrossRef]
10. Santos, P.F.; Niinomi, M.; Liu, H.; Cho, K.; Nakai, M.; Itoh, Y.; Narushima, T.; Ikeda, M. Fabrication of low-cost beta-type Ti-Mn alloys for biomedical applications by metal injection molding process and their mechanical properties. *J. Mech. Behav. Biom. Mat.* **2016**, *59*, 497–507. [CrossRef]
11. Bolzoni, L.; Ruiz-Navas, E.M.; Gordo, E. Influence of vacuum hot-pressing temperature on the microstructure and mechanical properties of Ti-3Al-2.5V alloy obtained by blended elemental and master alloy addition powders. *Mater. Chem. Phys.* **2012**, *137*, 608–616. [CrossRef]
12. Leyens, C.; Peters, M. *Titanium and Titanium Alloys: Fundamentals and Applications*; John Wiley & Sons: Köln, Germany, 2003.
13. Bolzoni, L.; Ruiz-Navas, E.M.; Gordo, E. Investigation of the factors influencing the tensile behaviour of PM Ti-3Al-2.5V alloy. *Mater. Sci. Eng. A* **2014**, *609*, 266–272. [CrossRef]
14. Kolli, R.; Devaraj, A. A review of metastable beta titanium alloys. *Metals* **2018**, *8*, 506. [CrossRef]
15. Bania, P.J. Beta Titanium alloys and their role in the titanium industry. *JOM* **1994**, *46*, 16–19. [CrossRef]
16. Wang, Q.; Dong, C.; Liaw, P.K. Structural stabilities of β-Ti alloys studied using a new Mo equivalent derived from [β/(α+ β)] phase-boundary slopes. *Metal. Mater. Trans. A* **2015**, *46*, 3440–3447. [CrossRef]
17. Chen, B.-Y.; Hwang, K.-S.; Ng, K.-L. Effect of cooling process on the alpha phase formation and mechanical properties of sintered Ti-Fe alloys. *Mater. Sci. Eng. A* **2011**, *528*, 4556–4563. [CrossRef]
18. Raynova, S.; Imam, M.A.; Yang, F.; Bolzoni, L. Hybrid microwave sintering of blended elemental Ti alloys. *J. Manuf. Proc.* **2019**, *39*, 52–57. [CrossRef]

19. Romero, C.; Yang, F.; Raynova, S.; Bolzoni, L. Thermomechanically processed powder metallurgy Ti-5Fe alloy: Effect of microstructure, texture, fe partitioning and residual porosity on tensile and fatigue behaviour. *Materialia* **2021**, *20*, 101254. [CrossRef]
20. Niu, J.; Guo, Y.; Li, K.; Liu, W.; Dan, Z.; Sun, Z.; Chang, H.; Zhou, L. Improved mechanical, bio-corrosion properties and in vitro cell responses of Ti-Fe alloys as candidate dental implants. *Mater. Sci. Eng. C* **2021**, *122*, 111917. [CrossRef]
21. Jirka, I.; Vandrovcová, M.; Frank, O.; Tolde, Z.; Plšek, J.; Luxbacher, T.; Bačáková, L.; Starý, V. On the role of Nb-related sites of an oxidized β-TiNb alloy surface in its interaction with osteoblast-like MG-63 cells. *Mater. Sci. Eng. C* **2013**, *33*, 1636–1645. [CrossRef]
22. Bai, Y.; Deng, Y.; Zheng, Y.; Li, Y.; Zhang, R.; Lv, Y.; Zhao, Q.; Wei, S. Characterization, corrosion behavior, cellular response and in vivo bone tissue compatibility of Titanium-Niobium alloy with low young's modulus. *Mater. Sci. Eng. C* **2016**, *59*, 565–576. [CrossRef] [PubMed]
23. Han, M.K.; Kim, J.Y.; Hwang, M.J.; Song, H.J.; Park, Y.J. Effect of Nb on the microstructure, mechanical properties, corrosion behavior, and cytotoxicity of Ti-Nb alloys. *Materials* **2015**, *8*, 5986–6003. [CrossRef] [PubMed]
24. Lee, C.M.; Ju, C.P.; Chern Lin, J.H. Structure-property relationship of cast Ti-Nb alloys. *J. Oral. Rehab.* **2002**, *29*, 314–322. [CrossRef] [PubMed]
25. Xu, L.J.; Xiao, S.L.; Jing, T.; Chen, Y.Y.; Huang, Y.D. Microstructure and dry wear properties of Ti-Nb alloys for dental prostheses. *Trans. Nonfer. Met. Soc. China* **2009**, *19*, s639–s644. [CrossRef]
26. Kikuchi, M.; Takahashi, M.; Okuno, O. Mechanical properties and grindability of dental cast Ti-Nb alloys. *Dental. Mater. J.* **2003**, *22*, 328–342. [CrossRef]
27. Xu, L.J.; Xiao, S.L.; Jing, T.; Chen, Y.Y.; Huang, Y.D. Microstructure and mechanical behavior of metal injection molded Ti-Nb binary alloys as biomedical material. *J. Mech. Behav. Biom. Mat.* **2013**, *28*, 171–182.
28. Yılmaz, E.; Gökçe, A.; Findik, F.; Gulsoy, H. Metallurgical properties and biomimetic HA deposition performance of Ti-Nb PIM alloys. *J. Alloy Comp.* **2018**, *746*, 301–313.
29. Kalita, D.; Rogal, Ł.; Czeppe, T.; Wójcik, A.; Kolano-Burian, A.; Zackiewicz, P.; Kania BDutkiewicz, J. Microstructure and mechanical properties of Ti-Nb alloys prepared by mechanical alloying and spark plasma sintering. *J. Mater. Eng. Perform.* **2020**, *29*, 1445–1452. [CrossRef]
30. Hsu, H.C.; Hsu, S.K.; Wu, S.C.; Lee, C.J.; Ho, W.F. Structure and mechanical properties of as-cast Ti-5Nb-xFe alloys. *Mater. Charact.* **2010**, *61*, 851–858. [CrossRef]
31. Ehtemam-Haghighi, S.; Liu, Y.; Cao, G.; Zhang, L.C. Phase transition, microstructural evolution and mechanical properties of Ti-Nb-Fe alloys induced by fe addition. *Mater. Des.* **2016**, *97*, 279–286. [CrossRef]
32. Afonso, C.R.M.; Chaves, J.M.; Florêncio, O. Effect of rapid solidification on microstructure and elastic modulus of β Ti-xNb-3Fe alloys for implant applications. *Adv. Eng. Mater.* **2017**, *19*, 1600370. [CrossRef]
33. Li, Q.; Miao, P.; Li, J.; He, M.; Nakai, M.; Niinomi, M.; Chiba, A.; Nakano, T.; Liu, X.; Zhou, K.; et al. Effect of Nb content on microstructures and mechanical properties of Ti-xNb-2Fe alloys. *J. Mater. Eng. Perf.* **2019**, *28*, 5501–5508. [CrossRef]
34. Chaves, J.M.; Florêncio, O.; Silva, P.S., Jr.; Marques, P.W.B.; Afonso, C.R.M. Influence of phase transformations on dynamical elastic modulus and anelasticity of beta Ti-Nb-Fe alloys for biomedical applications. *J. Mech. Behav. Biom. Mat.* **2015**, *46*, 184–196. [CrossRef] [PubMed]
35. German, R.M. *Powder Metallurgy and Particulate Materials Processing: The Processes, Materials, Products, Properties and Applications*; Metal Powder Industries Federation: Princeton, NJ, USA, 2005.
36. Raynova, S.; Collas, Y.; Yang, F.; Bolzoni, L. Advancement in the pressureless sintering of CP titanium using high-frequency induction heating. *Metal. Mat. Trans. A* **2019**, *50*, 4732–47422. [CrossRef]
37. Romero, C.; Yang, F.; Wei, S.; Bolzoni, L. Thermomechanical processing of cost-affordable powder metallurgy Ti-5Fe alloys from the blended elemental approach: Microstructure, tensile deformation behavior, and failure. *Metals* **2020**, *10*, 1405. [CrossRef]
38. Guo, S.; Meng, Q.; Zhao, X.; Wei, Q.; Xu, H. Design and fabrication of a metastable β-type titanium alloy with ultralow elastic modulus and high strength. *Sci. Rep.* **2015**, *5*, 14688. [CrossRef]
39. Ehtemam-Haghighi, S.; Prashanth, K.G.; Attar, H.; Chaubey, A.K.; Cao, G.H.; Zhang, L.C. Evaluation of mechanical and wear properties of TixNb7Fe alloys designed for biomedical applications. *Mater. Des.* **2016**, *111*, 592–599.
40. Bolzoni, L.; Alqattan, M.; Peters, L.; Alshammari, Y.; Yang, F. Ternary Ti alloys functionalised with antibacterial activity. *Sci. Rep.* **2020**, *10*, 22201.
41. Callister, W.D. *Fundamentals of Materials Science and Engineering*; Wiley: London, UK, 2000.
42. Nowak, M.; Yeoh, W.K.; Bolzoni LBabu, N.H. Development of Al-Nb-B master alloys using Nb and KBF_4 powders. *Mater. Des.* **2015**, *75*, 40–46. [CrossRef]
43. Jia, M.; Gabbitas, B.; Bolzoni, L. Evaluation of reactive induction sintering as a manufacturing route for blended elemental Ti-5Al-2. *5Fe alloy, J. Mat. Proc. Tech.* **2018**, *255*, 611–620. [CrossRef]
44. Boyer, R.; Welsch, G.; Collings, E.W. *Materials Properties Handbook: Titanium Alloys*; ASM International: Novelty, OH, USA, 1998.